# Relative control of domains' structure in Grain-Oriented electrical steels by Ultra-Short Pulsed laser ablation process

O. Maloberti, M. Nesser, E. Salloum, J. Dupuy, P. Dassonvalle, C. Pineau, S. Panier, J.P. Birat

# Relative control of domains' structure in Grain-Oriented Electrical Steels by Ultra-Short Pulsed Laser Ablation process

O. Maloberti[a,b,1], M. Nesser[b], E. Salloum[a,b], J. Dupuy[c], P. Dassonvalle[a,d], C. Pineau[e], S. Panier[b], J.P. Birat[f]

[a]*SYMADE-UNILASALLE Amiens, 14 quai de la Somme, Amiens, 80080, France ;* [b]*Laboratoire LTI, IUT d'Amiens Avenue des Facultés – Le Bailly, Amiens, 80025, France ;* [c]*Multitel a.s.b.l., 2 Rue Pierre et Marie Curie Parc Initialis, Mons, 7000, Belgique ;* [d]*Laboratoire MIS, UPJV, 14 quai de la Somme, Amiens, 80080, France ;* [e]*IRT-M2P, 4 rue Augustin Fresnel, Metz, 57070, France ;* [f]*IF Steelman, 5 rue du Gate-Chaux, 57280, Semécourt, France*

This paper investigates the impact of surface **U**ltra-**S**hort-**P**ulsed-**L**aser ablation process (**USPL**), mainly the groove depth, shockwave pressure and pattern, on magnetic characteristics of **G**rain-**O**riented **E**lectrical **S**teels (**GOES**) by using the **T**ensor **M**agnetic **P**hase **T**heory (TMPT). A sensitivity analysis to key laser parameters helps specifying the process thanks to a relative control of the surface magnetic structure (Magneto-Optical Indicator Film (MOIF)), dynamics and the behaviors (Single Sheet Tester (SST)) that follow.

*Keywords:* electrical steels, GOES, USPL, domains refinement, magnetization dynamics, iron losses, MOIF, SST.

## 1. Context and State of The Art

Surface laser treatment, first with Long Pulsed Lasers (LPL ≥ 10 ns) or continuous Wave Lasers (CWL), appeared as an elegant non-contact method [1-3]. Finally, different kinds of lasers in various pulse regimes were used more or less successfully [4, 5]. Recent research investigated advanced Short Pulsed (SPL < 10 ns) and Ultra-Short Pulsed Lasers (USPL < 10 ps) rather than LPL [6, 7]. The USPL process, called Ablation, creates deep grooves by vaporizing the coating and metal particles [8, 9]. Because each pulse is ultra short, its peak power is very high and this contributes to the generation of a plasma and a Laser Induced Shock Wave (LISW) underneath the groove [10]. The process control starts with models that estimate key pulsed laser impacts; and correlations with loss properties [11]. Reference [12] identified the LPL, SPL and USPL impacts on the Bertotti loss coefficients [13]. The present work contributes to the definition and optimization of key process parameters. Several specimens processed with various laser configurations are characterized thanks to both measurements and the TMPT model [14, 15].

## 2. Description of the Experiments

### 2.1. *Specimens: grades and dimensions*

One conventional grade of $Si_{w4\%}Fe_{w96\%}$ GOES named 23MXX with thickness $\zeta = 0.23$ mm, mass density $\gamma = 7400$ kg.m$^{-3}$, saturation polarization $J_s = 2.1$ T, specific losses $P_f = 0.95 \pm 0.05$ W/kg @1.5T50Hz measured with the SST, electrical conductivity $\sigma = 2$ MS.m$^{-1}$, ®carlite type coating of thickness 2 µm, will be investigated. Specimens used are squares with size 150*150 mm$^2$, laser treated on one or two sides with $N_P$ passes. One 1$^{st}$ experiment that aims at optimizing the process parameters uses 9 samples in (§3) and a second experiment dedicated to the laser pattern optimization uses 6 samples in (§4).

### 2.2. *Laser treatments and parameters*

The laser treatment is an USPL process performed with an Ytterbium Amplitude Laser at a wavelength of 1.03 µm with an adjustable pulse width $\tau_{pulse}$ [ps] between a few hundreds of fs and 10 ps with fixed spot diameter $\delta$ [µm] but various average powers, scanning speeds and repetition frequencies. This process also called laser ablation has been studied in references [8-12]. The main laser impacts necessary to qualify an USPL ablation in magnetics are the groove depth $p$ [µm] and the LISW peak pressure $\acute{P}$ [MPa] both relatively to mid reference values $p_n$ and $\acute{P}_n$, called nominal values close to optimal ones. Another important laser impact parameter is the product between $p$, the number of passes $N_P$ and $\acute{P}$, called $p\acute{P}$ [N.m$^{-1}$] and homogeneous to a mass acceleration [kg.s$^{-2}$], similar to a recoil effect of the particles ejected by the laser beam. One pattern with parallel lines perpendicular to the RD is investigated. The line spacing $d$ [µm] will be specified relatively to its nominal value $d_n$ as well.

### 2.3. *Methodology (MOIF, TMPT, SST)*

- *MOIF observations – magnetic structure analysis*

First, the magnetic domains at the samples surface are observed with the MOIF technique. More than 16 Images per configuration are analyzed with the 2D Fast Fourier Transform (FFT) to give the distribution probability density as a function of the space frequency $k$, inversely proportional to the domains width $w$.

- *TMPT Modeling – magnetic domains and properties*

The control of the process must connect the laser impacts with the magnetic domains' structure. The TMPT [14] has been proposed to statistically describe the domains and walls through a competition between a minimum of four energy terms at the mesoscopic scale. The total energy balance involves four material properties: the surface domains size, density and walls mobility lumped in $\Lambda_0$ [µm], a coercive reluctivity $\nu_c$ [m.H$^{-1}$] related to the grain boundaries and defects (giving the local static coercive field as a function

[1] * Corresponding author: olivie.maloberti@gmail.com

of flux density $B$), an anisotropic exchange characteristic $\kappa$ [mm$^{-2}$] (ratio between magnetic anisotropy plus magneto-striction and exchange properties) and finally the dynamic damping characteristic $\tau$ [µs] (closely dependent on the walls mobility and magnetization damping in the volume).

- *SST Magnetic measurements and identifications*

Identifications are possible by fitting the measurements along the Rolling Direction (RD), providing an accuracy better than 0.5% at high induction and 3% at low induction. The results include the changes in material characteristics *versus* the process parameters relatively to nominal values. Topological (domains size $w$, $\Lambda_0$ and structural $\kappa$ …), static and dynamical (coercive reluctivity $\nu_c$, walls mobility/damping delay $\tau$ …) properties of the magnetic structure are finally analyzed versus the same process parameters.

## 3. Impact of Groove depth $p$ and Laser Induced Shock Wave peak pressure $\acute{P}$

### 3.1. *Samples and process parameters*

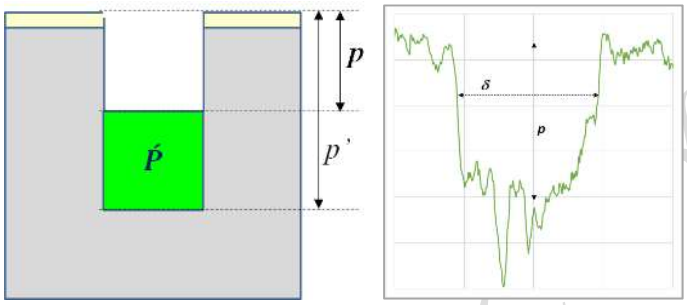


Fig. 1 : definition of groove depth $p$ & LISW pressure parameters $\acute{P}$ (left), confocal normalized image of one groove example (right)

In the first experiment we keep constant the laser spot size $\delta$ and line spacing $d$ and vary the process parameters such that it leads to various groove depth $p$. The groove depth has been measured and compared to an ablation estimation model [11, 12]. The way the groove is obtained also varies due to the energy of each single pulse $E_{pulse}$ [µJ] that determines its peak power. The cumulative energy that drives the quantity of material removed, *i.e.* the groove depth $p$, is given by $N \times E_{pulse}$, where $N$ is the number of pulses [8, 9]. The pulse peak power that drives the LISW peak pressure $\acute{P}$, is given by $E_{pulse}/\tau_{pulse}$ [MW]. Taking into account simultaneously the result of the engravement process (groove depth $p$ [µm]) and the way the groove is obtained (LISW peak pressure $\acute{P}$ [MPa] [10]) can be done by looking at the change in ablation speed of material mass removal per unit time: the ablation acceleration $p\acute{P}$ [kg.s$^{-2}$]. The list of samples used with the corresponding relative value of depth ($p/p_n$) and stress ($\acute{P}/\acute{P}_n$) is given in Table 1. Results associated to sample p0 correspond to an average of 16 standard samples with no laser.

Table 1 : Samples list for 1st (left) and 2nd (right) experiments

| samples | $p/p_n$ | $\acute{P}/\acute{P}_n$ |
|---|---|---|
| p0 | 0 | 0 |
| p125 | 0,125 | 0,61 |
| p187 | 0,187 | 0,26 |
| p250 | 0,250 | 0,64 |
| p375 | 0,375 | 1 |
| p625 | 0,625 | 1 |
| p1500 | 1,5 | 3,06 |
| p1625 | 1,625 | 1,53 |
| p2000 | 2 | 1,75 |
| p3000 | 3 | 3,06 |

| samples | $d/d_n$ |
|---|---|
| d0 | 0 |
| d167 | 0,167 |
| d333 | 0,333 |
| d667 | 0,667 |
| d1000 | 1 |
| d1333 | 1,333 |
| d1667 | 1,667 |

### 3.2. *MOIF observations and analysis*

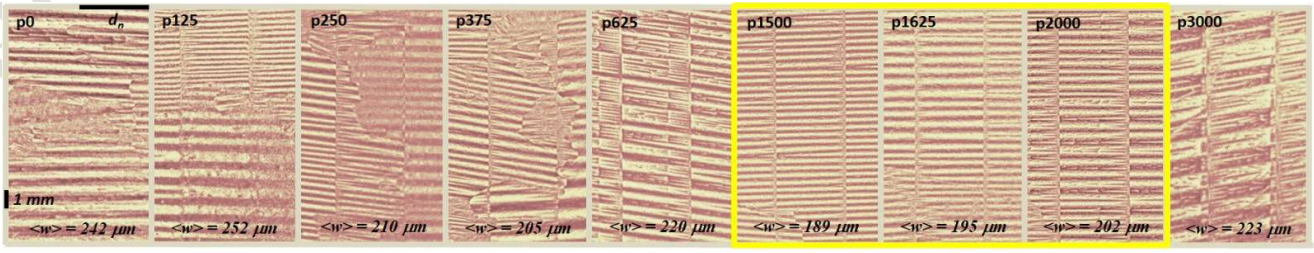


Fig. 2 : MOIF imaging of one representative location without/with a 2-sides, 1 or 2-passes Ablation varying the depth $p$ and pressure $\acute{P}$.

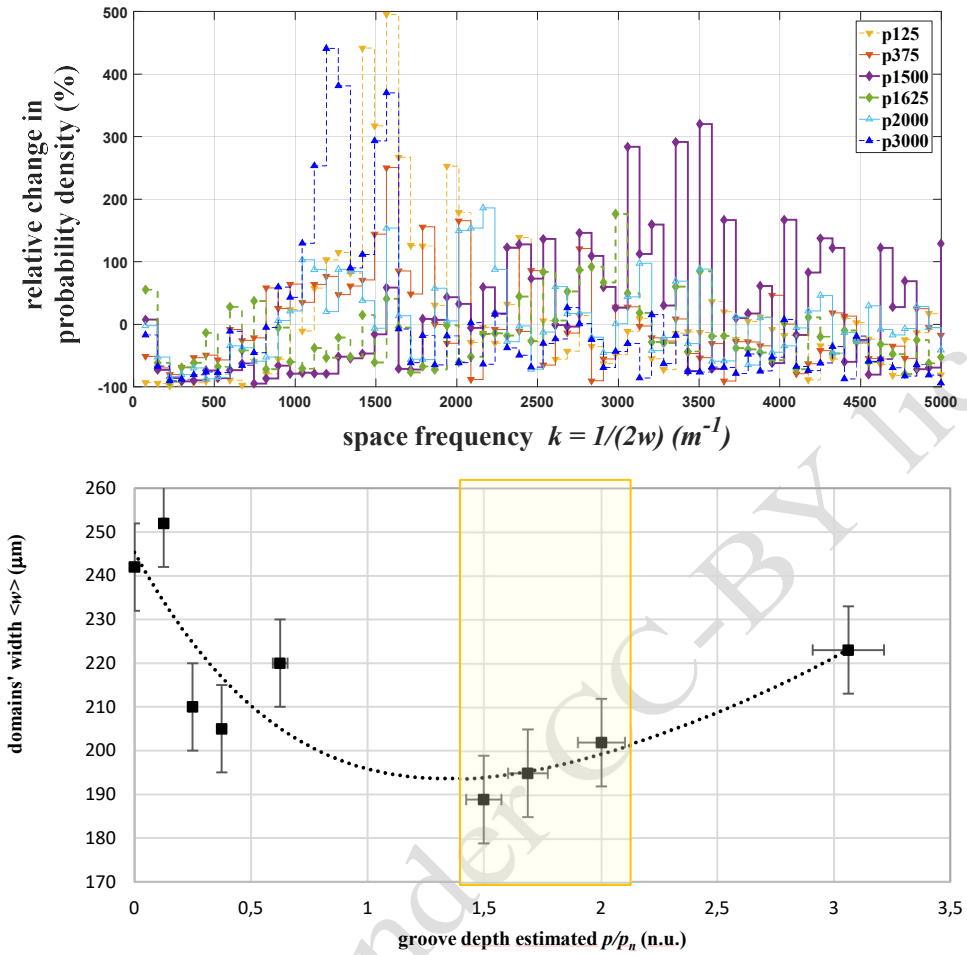


Fig. 3 : relative change of spatial probability density (left) and domains' width <*w*> (right) *versus* groove depth *p*.

Fig. 2 shows that the finest regular 180° domains are obtained for samples p1500 and p1625. This is confirmed with the probability density spectra of the domains' size in the Transverse Direction (TD) centred at higher space frequencies $k$ (Fig. 3). The highest $k$ values of those samples correspond to spike-like domains at the laser lines. Otherwise, the highest frequencies contain also Lancet and small 90° domains. The average width <*w*> is obtained with the median value $\bar{k}$ of spatial frequency $\langle w \rangle = 1/(n.S) = 1/(2\bar{k})$. The average domains width <*w*> reported in Fig. 3 shows a minimum value as a function of the groove depth $p$, when $1 < p < 2$. However, due to the LISW peak pressure effect, the optimal conditions for the iron losses does not depend only on this minimum domains' width with the groove depth but also on the impact of $\dot{P}$ on the domains and walls properties.

### *3.3. Magnetic measurements*

The whole nine samples of first experiment plus the 16 standard ones are measured with the SST to provide: $\mu_{app}$ [H.m$^{-1}$]: the apparent magnitude permeability, *i.e.* the ratio between the maximum induction level $B$ and the corresponding magnetic field $H$; $P_s$ [W.kg$^{-1}$]: the quasi static loss density measured as a function of $B$ @ $f$ = 3 Hz; $P_d$ [W.kg$^{-1}$]: the dynamic loss density measured at various $B$ and frequencies $f$; and $P_f = P_s + P_d$: the total iron losses. The relative variations found for the observables between laser treated and reference sample with no laser (average of 16 standard samples) as a function of the relative process parameter $(p\dot{P})/(p_n\dot{P}_n)=(p/p_n)(\dot{P}/\dot{P}_n)$ are reported in Fig. 4 for the specific working conditions $B$ = 1.5 T and $f$ = 50 Hz. The four parameters of the TMPT model detailed in [14, 15] can also be identified by fitting $\mu_{app}$, $P_s$ and $P_d$. The results of Fig. 4 show that a compromise between the static loss $P_s$ and the dynamic loss $P_d$ reduction factors is required. Providing $1 < p < 2$, the best reduction for $P_s$ occurs at low or high $p\dot{P}$ values when the best for $P_d$ is found for intermediate $p\dot{P}$. Therefore, for $B$ = 1.5 T and $f$ = 50 Hz, the minimum of total iron loss is found for $p\dot{P}$ from 2 to 5. Very low values of $p\dot{P}$ (<< 0.5) can provide significant reduction of $P_d$ but not of $P_s$ while decreasing $\mu_{app}$. This case altering the coating only looks like an irradiation or a scribing process [7, 11, 12]. $\mu_{app}$ can be increased only for average values of $p\dot{P}$ ($0.5 < p\dot{P} < 2$) and then quickly weakened while using stronger pulses with $p\dot{P} > 2$. Except for the limitation enforced by the sheet deformation above $p\dot{P} > 10$; deep grooves obtained with strong pulses can help only at sufficiently high frequencies $f \geq 50$ Hz for which $P_s$ is negligible and with a sufficiently low flux density $B \leq 1.9$ T when $\mu_{app}$ is not critically damaged.

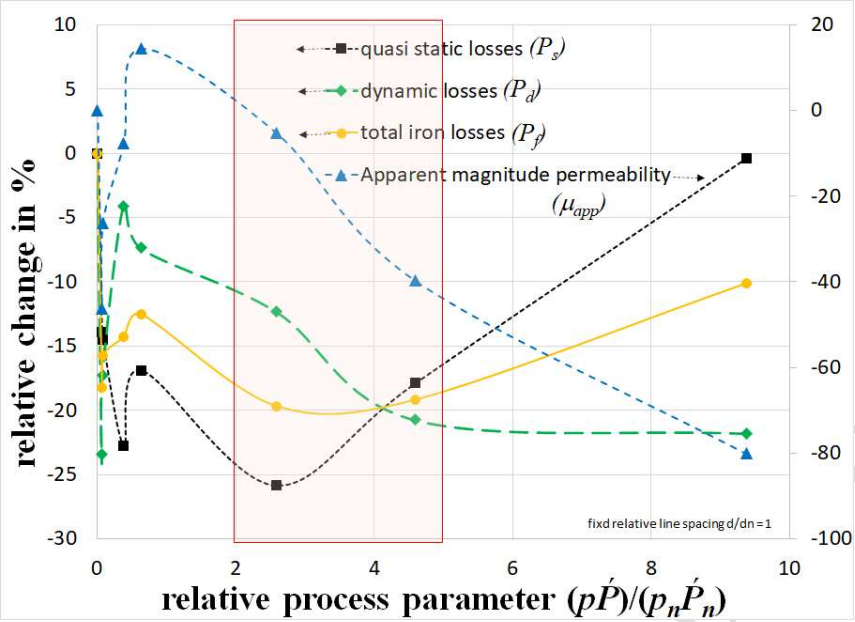


Fig. 4 : Magnetic results @1.5T@50Hz *v.s.* $pP\acute{}$.

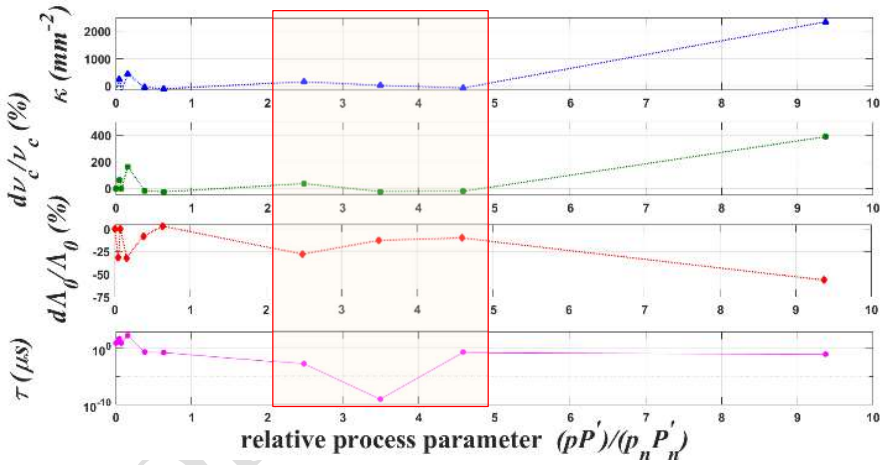


Fig. 5 : Variation of properties $\kappa$, $\nu_c$, $\Lambda_0$ and $\tau$ *v.s.* parameter $pP\acute{}$.

Looking at Fig. 5, tendencies are clarified with an increasing laser stress induced anisotropic exchange $\kappa$ at high $pP\acute{}$ values. The compromise between $P_s$ and $P_d$ is reproduced between $\nu_c$ and $\Lambda_0$. High values of $pP\acute{}$ are beneficial to reduce $\Lambda_0$ but also generate walls pinning spots which increases $\nu_c$. The lowered property $\Lambda_0$ is due to the surface domains refinement and dynamics. The damped magnetization in the volume involves a delay driven by the domains shape, size and $\tau$ which shows an optimal weakening, probably thanks to walls nucleation and multiplication sites, still for mid $pP\acute{}$ values ($2 < pP\acute{} < 5$).

## 4. Impact of line spacing *d*

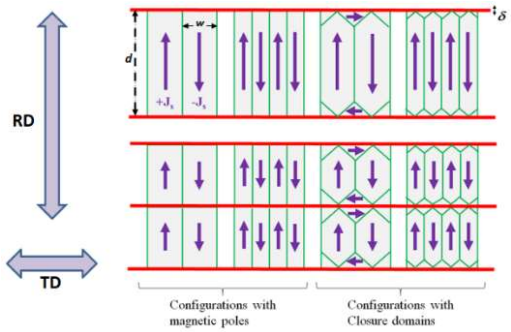


Fig. 6 : Line spacing *d* definition and impact.

In the second experiment, a very classical and well known pattern is studied (see Fig. 6): equidistant lines parallel to the Transverse Direction (TD) are engraved at both sides of each squared sample. We keep constant the laser spot size $\delta$ and the process parameters such that it leads to a fixed groove depth ($p/p_n$)=1.625 and a fixed LISW peak pressure ($\acute{P}/\acute{P}_n$)=1.53. We vary the pattern line spacing $d$ to analyze its impact on the magnetic losses and separate domains and walls properties. The list of samples used with the corresponding relative value of line spacing ($d/d_n$) is given in Table 1. The sample d0 is the same as sample p0 (§3.1).

### *4.1. MOIF observations and analysis*

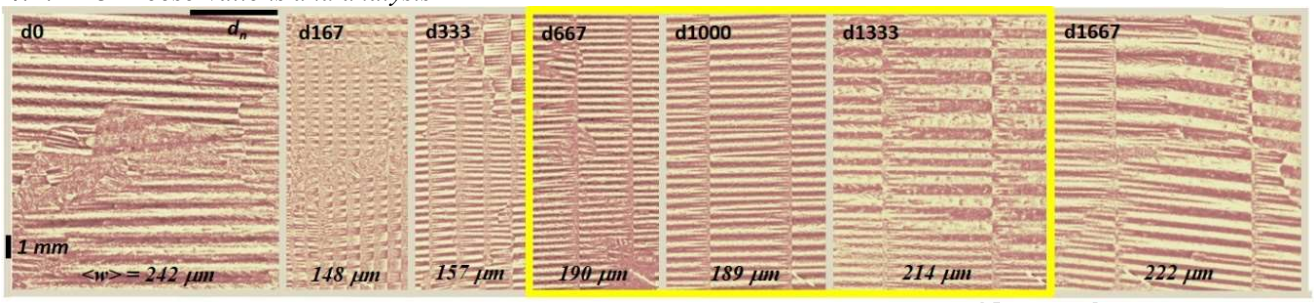


Fig. 7 : MOIF domains imaging of one representative location without/with a 2-sides and 1-pass Ablation process varying the line spacing $d$.

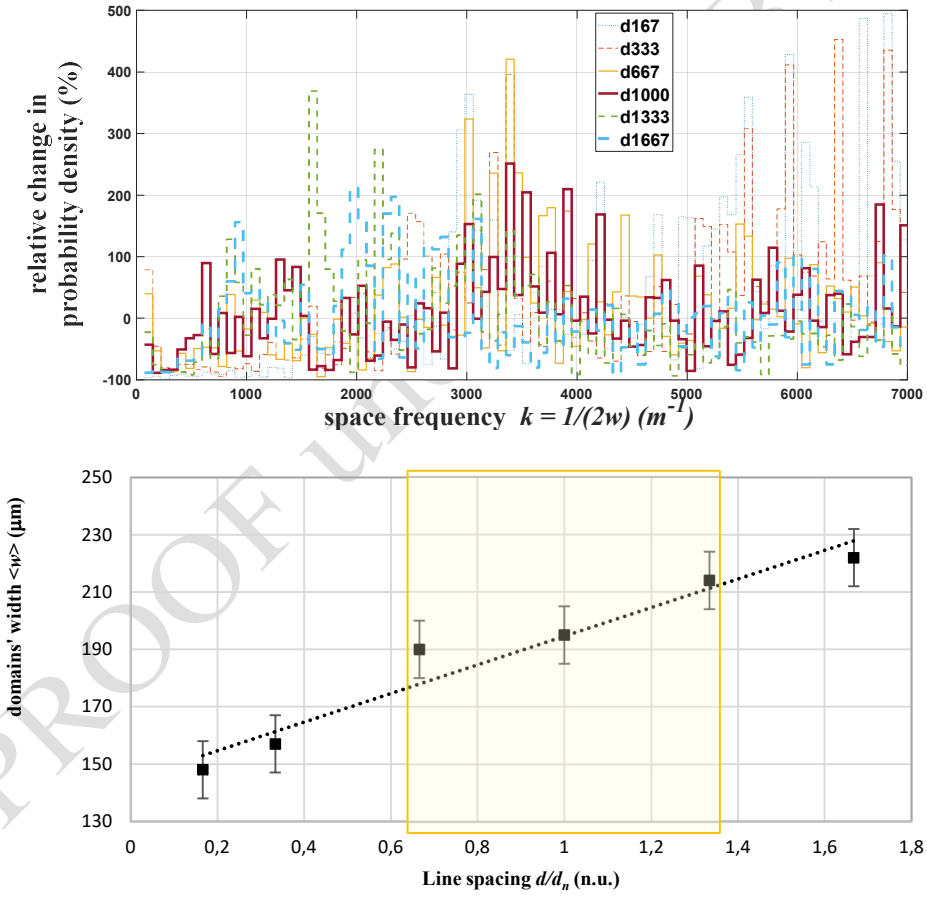


Fig. 8 : relative change of spatial probability density (left) and domains width $w$ (right) *v.s.* the line spacing $d$.

MOIF images of Fig. 7 show that the smallest domains are obtained for sample d167, *i.e.* for the smallest line spacing $d$. This is confirmed by analysing the average domains width <$w$> reported in Fig. 8 (right). <$w$> shows a monotonous increasing behaviour as a function of $d$. As expected, it will be shown in Fig. 9 that <$w$> is not the only criterion for the loss reduction: The walls mobility and damping, dependent on its density, plays an important role (Fig. 10). Logically, the median space frequency $k$ of the probability density spectra for the domains' size in the (TD) given in Fig. 8 (left) is also an increasing function of $d$. However, the median $k$ values of samples with the smallest line spacing $d$ are those of usual spike-like, Lancet and 90° domains. The latter imply laser induced stresses that for dense patterns can damage the permeability and lower the walls mobility with too high damping delays.

### *4.2. Magnetic measurements and identifications*

The whole six samples of second experiment plus the 16 standard ones are measured with the SST to provide $\mu_{app}$, $P_s$, $P_d$ and $P_f$. The best relative variations found for these four observables between each laser treated sample and the reference sample (average of 16 standard samples) as a function of the relative pattern parameter ($d/d_n$) are reported in Fig. 9 for the specific working condition $B$ = 1.5 T and $f$ = 50 Hz. The results obtained in Fig. 9 confirm that the size of domains cannot be the only criterion. For the smallest line spacings ($d/d_n$ < 0.75) and therefore the smallest magnetic domains, both the quasi static hysteresis losses $P_s$ and the apparent magnitude permeability $\mu_{app}$ are critically increased and damaged respectively. As a consequence, even if this fine patterns are able to reduce the dynamic losses $P_d$, it does not reduce but rather increases the total iron losses $P_f$. At the opposite situation with the highest line spacings ($d/d_n$ > 1.25), i.e. the largest domains, it is still possible to increase $\mu_{app}$ and reduce the quasi static part of losses $P_s$, but the reduction of dynamic $P_d$ and total $P_f$ losses becomes less efficient. To sum up, for $B$ = 1.5T and $f$ = 50 Hz, the minimum of total iron loss is found for ($d/d_n$) between 0.75 and 1.25, so close to the nominal 1. This area is the one with the maximum total loss reduction and the best compromise between the permeability and the loss improvements. As mentioned previously, this optimal configuration has been found for a process parameter $p\acute{P}$ range. A change in the process parameter might lead to more losses inside the optimal area defined for $d$, optimal area that should be shifted accordingly (see perspectives in §5). Except for the limitation enforced by the sheet deformation below $d$ < 0.25; closer lines can help only at sufficiently high frequencies $f \geq$ 50 Hz for which the static part is negligible and with a sufficiently low flux density $B \leq$ 1 T before the saturation knee.

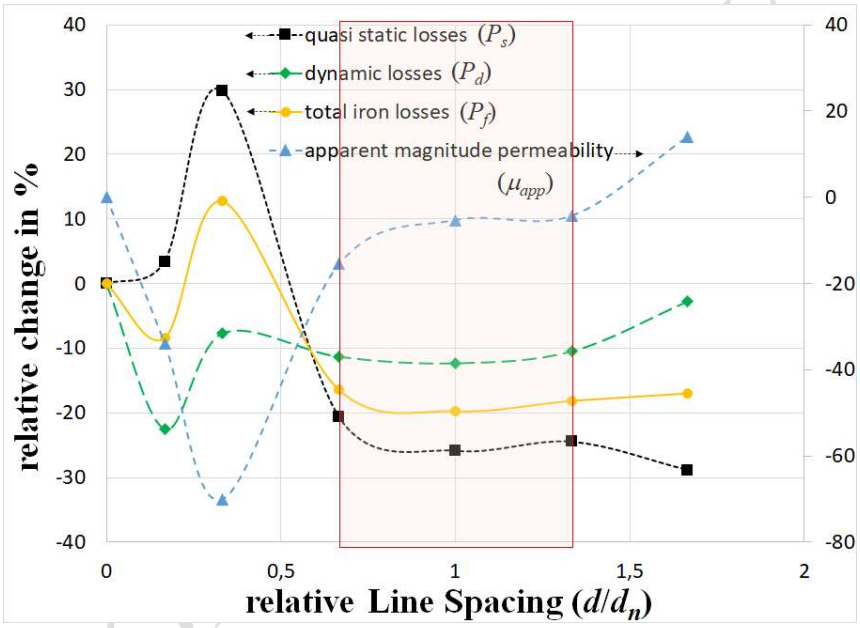


Fig. 9 : Magnetic results @1.5T@50Hz *v.s. d.*

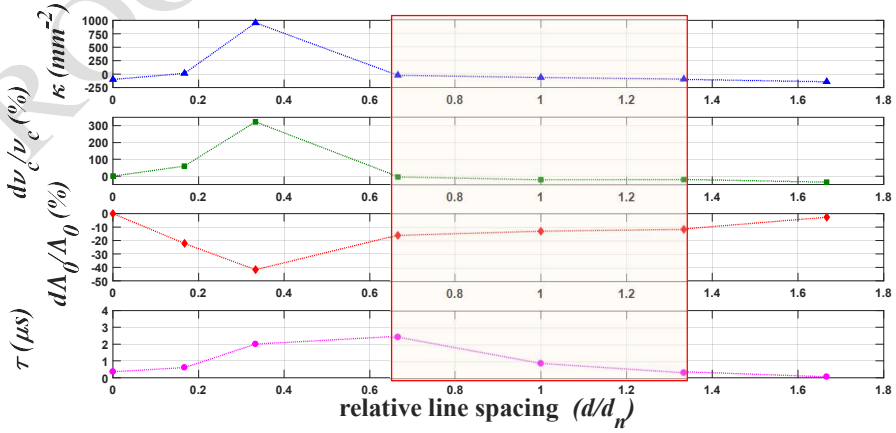


Fig. 10 : Variation of properties $\kappa$, $\nu_c$, $\Lambda_0$ and $\tau$ *v.s.* line spacing $d$.

Looking at Fig. 10, tendencies are clarified on the increasing laser stress induced anisotropic exchange $\kappa$ at small line spacings $d$. The compromise between $P_s$ and $P_d$ is reproduced between $\nu_c$ and $\Lambda_0$. Small line spacings $d$ are beneficial to reduce $\Lambda_0$ but it also generates

more walls pinning spots which make $\nu_c$ bigger. At small line spacings, the lowered property $\Lambda_0$ is accompanied by a more damped magnetization in the volume related to an increase of the delay $\tau$ probably due to congestion of walls at close grooves and between small domains not always well oriented. At optimal and higher line spacings $d$ the surface property $\Lambda_0$ can still be refined while keeping unaffected the delay $\tau$, meaning that the magnetization reversal mechanisms aren't damped with grooves sufficiently far from each other.

## 5. Conclusion and Perspectives

The optimal process and pattern parameters found thanks to the work of this paper are: $\boldsymbol{p/p_n}$ = 1.63; $\boldsymbol{\acute{P}/\acute{P}_n}$ = 1.53 and $\boldsymbol{d/d_n}$ = 1. Practically, this configuration allows to save an average maximum of 0.19 W/kg @1.5T@50Hz, reducing the total iron losses (basically the specific losses) from the average maximum 0.95 W/kg to the average minimum 0.76 W/kg. This technical solution is a compromise between:

- The inclusion of located laser spots – lines, that leads to : altered and stressed areas with reduction of polarization inside the affected zone ($\acute{P} \Rightarrow \kappa$ and $\mu_{app}$) / an increase of pinning – nucleation processes at engraved defects ($p \Rightarrow \nu_c$ and $P_s$).
- The induction of located closure domains or/and magnetic poles that defines the width of magnetic domains and the multiplication and mobility of walls driven by the total energy minimization ($d \Rightarrow \Lambda_0$, $\tau$ and $P_d$).

These results naturally lead to the following perspectives:

First, three process and pattern parameters have been studied either combined ($p\acute{P}=(p/p_n)(\acute{P}/\acute{P}_n)$) or separated ($d/d_n$) in order to find one optimal solution in a certain search space area. Not all the possible combinations have been reported in the present work and above all the next step consists in specifying the shifting rule of the optimal $d$-pattern area as a function of the $p$-process parameters. Then, among the process parameters, one has been put aside because it is not possible today either experimentally or theoretically to estimate correctly its value. In fact, the LISW penetration depth, named $p'$, has not been specified yet. This study will be the topic of another publication. Finally, The complete faithful microscopic description of magnetization reversal mechanisms requires to analyse further the dynamics of walls and domains in between and at the vicinity of the laser spots at the microscopic and the nanoscopic scales.

### References

[1] S. Patri, et al., Magnetic domain refinement of silicon-steel laminations by laser scribing, J. Mater. Sci., vol. 31, pp. 693-1702, 1996.
[2] Jingdong Li et al., J. of Mat. Proc. TechJ. Li, et al., Decreasing the core Loss of grain-oriented silicon steel by laser processing, J. Mat. Proc. Tech., vol. 69, pp. 180-185, 1996.
[3] S.V. Ponnaluri, et al., Core loss reduction in grain oriented silicon steels by excimer laser scribing – part I: Experimental work, J. Mat. Proc. Tech., vol. 112 (2-3), p. 199-204, 2001.
[4] Y. Huang et al., Int. J. Adv. Manu. Tech., vol. 70 (1-4), p. 1-9, 2014. ] Y. Huang, et al., Parameter optimization of Nd:Yag laser scribing process on core loss of grain-oriented magnetic silicon steels, Int. J. Adv. Manu., vol. 70 (1-4), p. 1-9, 2014.
[5] I. Petryshynets et al., AIP Adv., vol. 8, no 4, p. 047604, april 2018. I. Petryshynets, et al., Magnetic losses reduction in grain oriented silicon steel by pulse and continuous fiber laser processing, AIP Adv., vol. 8, no 4, p. 047604, april 2018., https:// doi.org/10.1063/1.4994191.
[6] J. Dupuy et al., SPIE LASE conf., Proc. vol. 10911, 2505326, 2019. J. Dupuy, et al., Comparison between laser thermal effects and ablation effects with ultrashort pulsed laser on GO SiFe electrical steel, SPIE LASE conf., Proc., vol. 10911, 2505326, 2019.
[7] M. Nesser et al., EJEE, vol. 23, n°6, Dec. 2021, pp. 439-444. M. Nesser, et al., Influence of a laser irradiation and laser scribing on magnetic properties of GO silicon steels sheets using a nanosecond fiber laser, EJEE, vol. 23, n°6, Dec. 2021, pp. 439-444.
[8] B.N. Chichkov, et al., Femtosecond, picosecond and nanosecond laser ablation of solids, A.P. Mat. Sci. Proc., vol. 63 (2), p. 109-115, 1996., https://doi.org/10.1007/ BF01567637.
[9] K. H. Leitza et al., *Phys. Procedia*, vol. 12, p. 230-238, 2011. K.H. Leitza, et al., Metal Ablation with Short and Ultrashort Laser Pulses, Phys. Procedia, vol. 12, p. 230-238, 2011, https://doi.org/10.1016/j.phpro.2011.03.128.
[10] P. Peyre et al., *Opt. Quant. Elect.*, vol. 27, p. 1213-1229, 1995. P. Peyre, et al., Laser shock processing: a review of the physics and applications, Opt. Quant. Elect., vol. 27, p. 1213-1229, 1995, https://doi.org/10.1007/BF00326477.
[11] Nesser, et al., Correlation between laser energetic parameters and magnetic properties of GO laminations under surface treatments with long, short or ultrashort pulsed lasers, J. Magn. Magn. Mater, vol. 504, 15 June 2020, 166696.
[12] M. Nesser et al., IEEE Trans. on Mag., vol. 58 (8), 2001105, 2022 M. Nesser, et al., Impact of Ultra-Short Pulsed Laser (USPL) Ablation Process on Separated Loss Coefficients of Grain Oriented Electrical Steels, IEEE Trans. Mag., vol. 58 (8), 2001105, 2022, https://doi.org/10.1109/TMAG.2022.3152899.
[13] G. Bertotti, et al., General properties of power losses in soft ferromagnetic materials, IEEE Trans. Mag., vol. 24, 1988, p.621-630, https://doi.org/10.1109/ 20.43994.
[14] O. Maloberti, et al., The Tensor Magnetic Phase Theory for mesoscopic volume structures of soft magnetic materials – Quasi-static and dynamic vector polarization, apparent permeability and losses – Experimental identifications of GO steel at low induction levels, J. Magn. Magn. Mater 502 (2020) 166403.
[15] O. Maloberti, et al., Discriminating the physical impacts of various laser pulses on the magnetic structure of oriented electrical steels, J. Magn. Magn. Mater, vol. 502, may 2020, 166403, 170248. ISSN 0304-8853, https://doi.org/10.1016/j.jmmm.2022.170248.

### Acknowledgements

This research has received funding from the European Research Council under the H2020-IND-CE-2016-17/H2020-FOF-2017 Program (Grant No. 766437).